Thermal electron emission from the hot electronic subsystem of vibrationally cold C_{60}

K. Hansen
Department of Experimental Physics, Gothenburg University and Chalmers University of Technology, SE-41296 Gothenburg, Sweden

K. Hoffmann[a)]
Max Born-Institut für Nichtlineare Optik und Kurzzeitspektroskopie, Max-Born-Str. 2a, D-12489 Berlin, Germany

E. E. B. Campbell
Department of Experimental Physics, Gothenburg University and Chalmers University of Technology, SE-41296 Gothenburg, Sweden

(Received 26 March 2003; accepted 30 April 2003)

We compare theoretical results on statistical electron emission from electronically hot but vibrationally cold C_{60} with recent experimental results involving excitation with ultrashort laser pulses. Both photoelectron spectra and ion yields of C_{60} as well as fragment ions are compared with the predictions of the statistical electron emission model. Quantitative agreement is obtained between the calculations and the experimentally measured photoelectron spectra, total ion yields and singly-doubly charged branching ratio. The electron-phonon coupling time is fitted to a few hundred femtoseconds, consistent with independent measurements. The data allow a determination of the thermal properties of the electron system, which are consistent with the theoretical input. The data also allow a fit of the averaged photon absorption cross section. © *2003 American Institute of Physics.* [DOI: 10.1063/1.1584671]

I. INTRODUCTION

The study of the photoionization of fullerenes has led to many interesting and occasionally unexpected results. One of the early observations made when exciting fullerenes with ns laser pulses was the delayed ionization of the neutral molecule on a microsecond time scale.[1] This can be interpreted in terms of statistical, thermionic emission of electrons from the vibrationally hot molecule and has been observed from many systems where the electron detachment energy is sufficiently far below the dissociation energy.[2–5] Recent experiments using femtosecond laser pulses have shown very different ionization behavior as the excitation time scale is varied from 25 fs to 5 ps.[6] For very short laser pulses ($<$70 fs), the ionization is predominantly via direct multiphoton ionization showing above threshold ionization. For intermediate pulse durations, of particular interest here, the ionization is predominantly statistical but without strong vibrational heating of the molecule and, finally, for pulse durations beyond a few hundred femtoseconds the thermionic microsecond delayed ionization begins to appear.[7]

In this paper we present a theoretical model of the statistical electron emission from C_{60} in the intermediate ionization regime and compare it with detailed experimental results on the laser pulse duration and fluence dependence of C_{60} photoelectron spectra and ion mass spectra. The model was presented in Ref. 8 and used in Ref. 9 to account for the electron yield in Penning ionization of C_{60}. This work provided the inspiration for the initial laser pulse duration studies and allowed an interpretation of the electron kinetic energy spectra.[6] Ionization yields and photoelectron spectra from sodium cluster ions excited with fs laser pulses have also been interpreted in terms of this picture.[10,11] The idea of transient electron heating of small particles has also been used in a somewhat different context,[12] viz. to interpret pump-probe spectra of copper and silver nanoparticles embedded in a transparent matrix and has been used on a number of other occasions to describe the short time dynamics of both clusters and surfaces (see, e.g., Refs. 13, 14).

The model presented here uses an improved calculation of the electronic density of states of C_{60} compared to the earlier version.[9] The Penning ionization data from two different groups[9,15] is used to independently fit the adjustable parameter in the calculations—the time constant for the coupling of electronic to vibrational excitation. We show that the value obtained from the Penning ionization data is consistent with femtosecond photoionization data. The model can satisfactorily reproduce the dependence of the photoelectron spectra on laser fluence in addition to several observable quantities related to the yield of positive ions. This is done using just one fit parameter, the average photon absorption cross section, which is determined to be 0.04 Å^2, with a factor of two uncertainty on the mean value.

II. TRANSIENT THERMAL ELECTRON EMISSION FROM C_{60}

The experimental data show evidence for four distinct ionization mechanisms, depending on the excitation time

[a)]Present address: Department of Physics, Texas University, Austin, Texas 78712.

scale and laser intensity. For very short excitation times (<70 fs) the ionization is dominated by direct, prompt multiphoton ionization accompanied by above threshold ionization (ATI).[6] For intensities greater than ca. 10^{14} W/cm^2 this is replaced by tunnel ionization.[16] For excitation time scales on the order of 100 fs, the electron emission is thermal in nature although the ionization occurs promptly on the time scale of time-of-flight mass spectrometry (<100 ns) and multiple ionization may occur. This is the region of interest in the present work. This situation then gradually (on the ps time scale)[7] develops into the more familiar delayed electron emission (thermionic emission) from vibrationally hot C_{60} where the excitation energy resides mainly in the vibrational degrees of freedom, and thermal electrons are emitted up to many microseconds after excitation.

The electron spectra and the ionization yields are described in terms of a model which postulates an intermediate state between the photon absorption and the complete dissipation of the excitation energy in the molecule. In this intermediate state the electrons can be considered hot and the vibrational degrees of freedom cold.[8,9] The short-time electron emission occurs from the incoherently excited electronic subsystem with the ionic degrees of freedom playing no active role but only acting as a thermal sink. One may introduce an equilibration time for the electrons between excitation and the totally equilibrated electron system, as described in, e.g., Ref. 17, but at no point in the analysis did we find any strong suggestions that it is needed to describe electron emission from C_{60}. This agrees with the experimental observations in Ref. 17, where the equilibration time was found to decrease with the radius of the particle. The results of Ref. 6 also indicate that the emission is statistical after at most 100 fs. The disappearance of the ATI peaks at longer pulse durations only sets an upper limit to the equilibration time. The electron-electron equilibration time may still be significant relative to the shortest relevant rate constants and could possibly have an influence on the value of the fitted photon absorption cross section. This will be discussed in the discussion and conclusion section of the paper.

In Ref. 9 the measured quantity was the total yield of ions which was quenched on the ps time scale by coupling to the thermal sink of the nuclear degrees of freedom. The coupling is characterized by a time constant which was fitted to about a picosecond. The fit of this time constant required an expression for the emission rate and, since the model is statistical, also an expression for the electronic level density of C_{60} and C_{60}^+. The rate constant reads[18,19]

$$k(E,\varepsilon)d\varepsilon = \frac{2m_e\sigma(\varepsilon)}{\pi^2\hbar^3}\varepsilon\frac{\rho_d(E-\Phi-\varepsilon)}{\rho_p(E)}d\varepsilon. \tag{1}$$

Here ε is the kinetic energy of the electron, m_e the mass of the electron (in principle the reduced mass of the channel), ρ the level density and Φ the ionization energy. The values used are 7.6 eV for the first *IE* (for neutral C_{60}), 11.4 eV for the second, 16.6 eV for the third, and 20 eV for the fourth. The factor of 2 in Eq. (1) is the spin degeneracy of the electron and $\sigma(\epsilon)$ is the capture cross section for an electron in the Coulomb potential of the daughter. The ρ's are the level densities of the daughter and the parent molecule, as indicated by the subscripts. The total rate is:

$$k(E) = \int_0^E (E,\varepsilon)d\varepsilon. \tag{2}$$

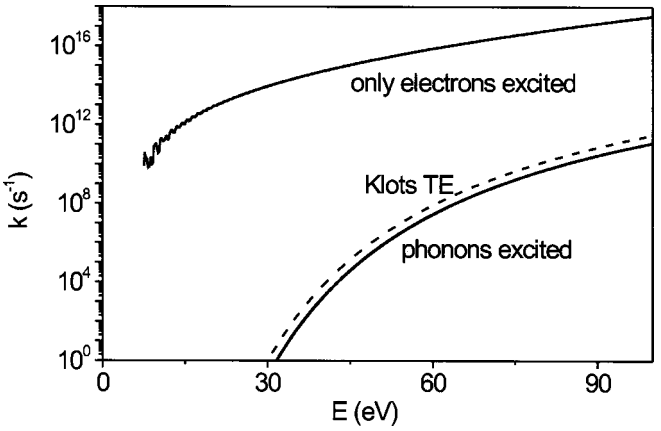

FIG. 1. Thermal electron emission rate for C_{60} when (a) all excitation energy resides in the electronic excitations, and (b) the excitation energy is equilibrated into the vibrational degrees of freedom. The large ratio between the two rates illustrates the strong quenching of the emission when the excitation energy is transferred from purely electronic excitations to vibrational excitations.

The rate constant in Eq. (1) is shown in Fig. 1 together with the rate constants expected when the excitation energy is distributed over the vibrational degrees of freedom, with an expression identical to Eq. (1), except for the different density of states.[19] Both are for ionization of the neutral molecule. The electronic level densities are specified below. The vibrational level density was calculated with the Beyer-Swinehart algorithm and vibrational frequencies from Ref. 20. For comparison we also show a frequently used rate equation for thermionic emission given by Klots.[21]

Apart from electron emission, coupling to the nuclear motion is the main damping mechanism of the electronic excitations. Radiative cooling plays a minor role. A calculation of the frequency integrated photon emission rate gives a value of 8×10^9 s^{-1} for a temperature of 1 eV and a photon absorption cross section of 100 Å^2. The finite heat bath correction[22] and the correction for stimulated emission[5] is ignored in this calculation but those are relatively minor corrections here. Radiative cooling can therefore safely be ignored at ps time scales.

When the laser fluence is low enough to cause only singly ionized species to appear the electron and ion yields are identical and equal to

$$Y = 1-\exp\left(-\int_0^\infty k(E(t))dt\right). \tag{3}$$

For small yields the expression can be approximated by expanding the exponential and this procedure was used in Ref. 9. In this work we will retain the exponentiated expression throughout when calculating yields since they may approach unity for the higher excitation energies of relevance here.

The dissipation is assumed to have an exponential time dependence, $E=E_0\exp(-t/\tau)$. This is close, but not identical, to the two-temperature model which is frequently used in the interpretation of experiments of transient optical properties of deposited clusters and surfaces probed by sub-ps lasers. One difference is the formulation here in terms of the electronic excitation energy and not the electronic temperature. This must be preferred when one works with small excitation energies where the discrete level structure of the molecule plays a role. Other differences between the coupling schemes are minor, as for example the temperature dependence of the coupling constant in the two-temperature model, which is a result of the energy/temperature dependent electronic heat capacity and which does not appear when the coupling is formulated in terms of energy. It should be noted, however, that the definitions of the coupling constants differ for the two formulations.

Introducing the time dependent electronic excitation energy into the yield equation gives

$$Y=1-\exp\left(-\int_0^\infty k(E_0e^{-t/\tau})dt\right). \tag{4}$$

The value of τ can be fitted from energy resolved measurements of the yield once the level densities and the capture cross section in Eq. (1) are specified. In Ref. 9 the level densities were not calculated explicitly. Instead the rate was cast in a form where a microcanonical temperature was used. This was done in order to take into account the HOMO-LUMO gap for the neutral C_{60}. The parameters were adjusted to agree with the low and high temperature limits of the expected behavior of a Fermi gas with the specific features that characterize the low energy excitation spectrum of C_{60}. The yield, and therefore also the fitted value of τ, is sensitive to the choice of this function, as already noted in Ref. 8. It is therefore desirable to have a better estimate of the level density. *Ab initio* calculations of the huge number of excited states involved are obviously out of the question and we have therefore used the single particle ground state spectrum from a Local Density Approximation calculation[23] as the basis for a calculation where the excitation spectrum is composed of particle-hole excitations. The single particle spectra for the cations were taken to be identical to that of the neutral, the only difference in the calculation being the number of electrons. The details of the algorithm, which calculates total level densities from the single particle spectrum, are given in the Appendix. Although numerically exact within the chosen resolution of 0.02 eV the algorithm cannot be expected to provide the true excitation spectrum for several reasons. One is that excited states can in principle not be calculated from the ground state solution of the LDA. Another is that the states are assumed to have vanishing widths which contradicts the treatment of the excitations as being thermal on the sub-ps timescale. Although we are not able to give rigorous limits, we do not expect the first defect to cause any serious modifications of the excitation spectrum at high energy where the density of states is high. The lifetime broadening may have an effect, in particular on the electron energy distributions, since the lifetimes approach values comparable with the inverse electron temperature. This suggests that the level density may need to be modified, but we will not do this here. Finally the Rydberg states, a few of which are observed experimentally,[24] are absent in the calculated spectrum. Although they will contribute to the density of states their number will be limited by an effective decoupling of the states with lifetimes longer than τ.

To estimate the capture cross section of the inverse process, we use the classical value for an electron in a Coulomb potential for distances larger than the fullerene radius and absorption when the electron reaches the edge of the fullerene. The experimental justification for this choice is the photoelectron kinetic energy spectrum measured for conventional thermionic emission from vibrationally hot fullerenes[25] which is consistent with this cross section. The measured spectrum agrees well with the one calculated with similar assumptions as those used here. No direct experimental measurement of the capture cross section is available for the very high electron energies relevant here. However, even for the relatively very low temperatures of molecular beams (700–800 K) measurements of electron attachment to the neutral molecule give values which correspond to a sticking coefficient of 0.1 (see Ref. 26 for an example and Ref. 5 for a review of several experiments). For the Coulomb potential and at the much higher temperature of interest here (typically 10^4 K), where the phase space for electron-electron scattering is so much higher, it is not unreasonable to expect a sticking coefficient approaching unity. Adopting that value yields a capture cross section of

$$\sigma(\varepsilon)=\pi r_0^2(1-V(r_0)/\varepsilon). \tag{5}$$

We use the value $V(r_0)=-e^2/4\pi\varepsilon_0 r_0=-3.0$ eV as in Ref. 9.

The experimental data used for the fit were the combined set of data on Penning ionization yields of Weber *et al.*[9] and Brunetti *et al.*[15] The latter provides only relative values but adds a point at low energy, for Xe, at 8.32 eV, i.e., only 0.74 eV above the ionization energy of C_{60}. The two data sets agree very well where identical energies have been measured and the data of Ref. 9 have therefore been used as normalization for the yields of Ref. 15.

We have allowed a small variation of the daughter level density to optimize the fit of the yields. With the form $\rho_d(E)=\rho_{d,\mathrm{calc}}(E)^{1+\alpha}/\rho_{d,\mathrm{calc}}(20\ \mathrm{eV})^{\alpha}$ for the singly charged cation and the neutral molecule level density unchanged, the best fit of τ was 240 fs, with the choice $\alpha=0.12$. The fitted value of τ is confirmed by independent pump–probe experiments[27] and also agrees with measurements of the time dependence of photoelectron kinetic energy spectra (see Sec. IV B). The result of the fit of the Penning ionization data is shown in Fig. 2 together with the measured yields. The value of τ obtained from the fit is smaller than the one pertaining to the postulated level density in Weber *et al.*[9] by a factor of 6. We believe that the 240 fs is closer to the true value, mainly based on the experimentally measured characteristic time, and will adopt this value in the following.

III. EXPERIMENTAL PROCEDURE

The experimental apparatus has been described previously.[6,28] It consists of three differentially pumped

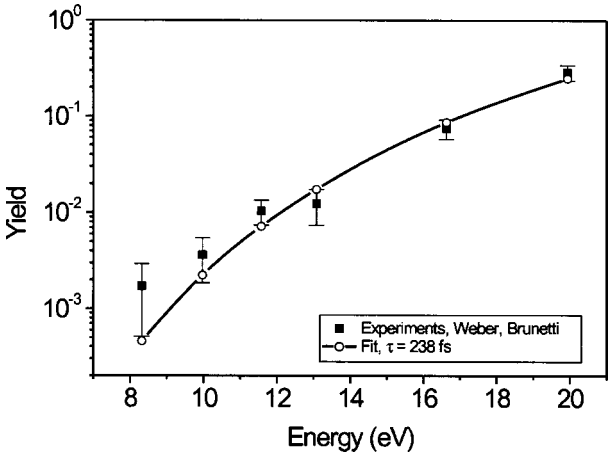

FIG. 2. Measured Penning ionization yields from Refs. 9, 15 and the calculated yield as a function of the metastable rare gas atom energy. The yield is calculated with Eq. (4).

vacuum chambers. The central chamber contains the fullerene source and is also where the laser interaction takes place. On either side of the extraction region there are a time-of-flight mass spectrometer for detection of positive ions and a time-of-flight photoelectron spectrometer. The positive ions are extracted with an electrostatic field. The photoelectrons are allowed to travel under field-free conditions to the electron detector. It is not possible to detect positive ions and photoelectrons simultaneously, however, it is possible to quickly switch between the two detection modes so that positive ions and electrons can be detected under identical excitation conditions. The excitation source was a Ti:sapphire regenerative amplifier system (800 nm) providing a bandwidth limited pulse duration of 180 fs ($\Delta E \approx 10$ meV). The pulse duration was extended by detuning the compressor, thereby keeping the bandwidth constant. The C_{60} molecular beam was produced from purified "gold grade" C_{60} powder heated in an oven to a temperature of 500 °C. The laser beam was perpendicular to both the C_{60} beam and the axes of the two spectrometers. Xe was used to calibrate both the electron spectrometer and the laser intensity. The Gaussian laser beam was focused with a 30 cm lens into the interaction region to form a spot radius of ca. 25 μm. The laser intensity was adjusted using a series of neutral density filters. The photoelectron spectra reported here were integrated over 50 000 laser shots at a 1 kHz repetition rate. The mass spectra were normally integrated over a lower number of laser shots, typically 5000–10 000.

IV. RESULTS

A. Electron kinetic energy spectra

For a certain electronic excitation energy, E_0, the electron kinetic energy distribution is given by Eqs. (1) and (5):

$$P(E_0,\varepsilon) \propto (\varepsilon + |V(r_0)|) \frac{\rho_d(E_0 - \Phi - \varepsilon)}{\rho_p(E)}. \tag{6}$$

Since the hot electronic system is assumed to cool continuously, the excited fullerenes will emit electrons with varying distributions during the whole quenching time. The distribution integrated over time is given by

$$P_{\text{int}}(E_0,\varepsilon) \propto \int_0^\infty (\varepsilon + |V(r_0)|) \frac{\rho_d(E_0 e^{-t/\tau} - \Phi - \varepsilon)}{\rho_p(E_0 e^{-t/\tau})} \times \exp\left(- \int_0^t k(E_0 e^{-t'/\tau}) dt' \right) dt, \tag{7}$$

where E_0 is the total photon energy absorbed, and $E_0 \exp(-t/\tau)$ is the electronic excitation energy at time t. The last exponential factor in the integrand takes the depletion of the population by electron emission into account.

These distributions, predicted for the case of a single well-determined initial energy of E_0, are therefore those expected for, e.g., the Penning ionization processes[9,15] where the excitation energy is well-defined. For photoexcitation experiments the distributions need to be integrated also over the distribution of absorbed photons. For a given fluence, F, we will assume a Poisson distribution with a mean λ given by the product of the fluence and the photo absorption cross section, σ_{ph}, divided by the photon energy, i.e., $\lambda = F\sigma_{ph}/h\nu$. In the present case $h\nu = 1.55$ eV. Also the fluence has a distribution which must be considered. The laser beam is known to be well represented by a Gaussian profile and the distributions must be averaged over this profile. Summing over photon numbers absorbed and the beam profile yields:

$$P_{\text{obs}}(\varepsilon) \propto \int_{r=0}^\infty dr\, r \sum_{n=0}^\infty P_{\text{int}}(nh\nu,\varepsilon) \times \frac{((\sigma_{ph}F_0/h\nu)e^{-(r/r_0)^2})^n}{n!} e^{-(\sigma_{ph}F_0/h\nu)e^{-(r/r_0)^2}}. \tag{8}$$

Introducing the expression for P_{int} gives the result:

$$P_{\text{obs}}(\varepsilon) \propto \int_{r=0}^\infty dr\, r \sum_{n=0}^\infty \int_0^\infty (\varepsilon + |V(r_0)|) \times \frac{\rho_d(nh\nu e^{-t/\tau} - \Phi - \varepsilon)}{\rho_p(nh\nu e^{-t/\tau})} \times \frac{((\sigma_{ph}F_0/h\nu)e^{-(r/r_0)^2})^n}{n!} e^{-(\sigma_{ph}F_0/h\nu)e^{-(r/r_0)^2}} \times \exp\left(- \int_0^t k(nh\nu e^{-t'/\tau}) dt' \right) dt. \tag{9}$$

Although not simple, this expression does not contain any new fit parameters, provided the laser beamwaist r_0 is independent of the peak fluence, F_0, and that the neutral molecular beam is homogeneous across r_0. The precise value of r_0 is not of importance here since it can be scaled away and hence only gives rise to an overall multiplicative factor. We will not consider this normalization to get the absolute yield since it was not measured experimentally.

Only the yield from the singly ionized species is included in Eq. (9). It will be clear from the calculation below

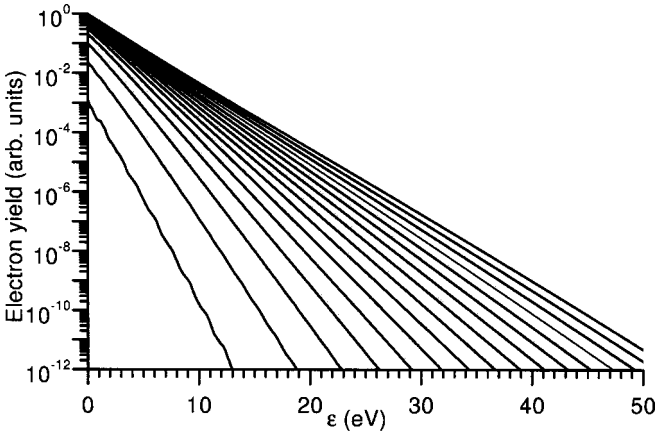

FIG. 3. Electron energy distributions calculated according to Eq. (9) and the similar contributions from ionization of higher charge states. The distributions correspond to an average number of 5, 10, 15, ..., 80 photons of 800 nm absorbed in the center of the laser beam.

of double ionization that the electron energy distributions will begin to receive contributions from second ionized molecules below the fragmentation limit, e.g., an average number of 15 absorbed photons give a 10% contribution from the second ionization. This contribution and the one from the third ionization must therefore be added before one can compare the simulations with the experimental data. This will be done in the following unless explicitly stated. The contribution of the second and higher ionization is calculated with a rate which is analogous to the expression Eq. (6) and a time dependence similar to Eq. (7). The only difference is that the value of $V(r_0)$ is n times the value of the first ionization for the daughter cluster with charge $n+$, and that the ionization energies, Φ, change (increase). The ensuing modifications of the yield equation, Eq. (9), are not difficult to implement in numerical calculations, but gives a very unwieldy formula which we will not show. One important property survives: The result still does not contain any fit parameters, as Eq. (9). The effect of including the higher charge states in the calculation is minor compared with the effects of the averaging implied in Eq. (9).

Calculated electron energy distributions are shown in Fig. 3 for several different values of E_0. The curves include the contribution from the doubly and triply ionized species. The main effect of the averagings and the time integration in Eq. (9) is to make the electron yield curve resemble a pure exponential more closely compared to the distribution obtained without these complications, mainly by adding low energy spectra to the average which reduces the negative curvature of the logarithm of the yields. The low energy part of the spectrum is still flatter than the observed spectrum but this discrepancy is caused predominantly by the presence of Rydberg peaks in the experimental data[24] which are not taken into account in this model. Only the electron spectra above 2 eV should and will be used for comparison with the calculations to avoid this complication.

Figure 4 shows examples of the comparison between experimental distributions, measured for a laser pulse duration of 180 fs, and calculated distributions. The labeling of the theoretical curves with λ_0 indicates the mean number of

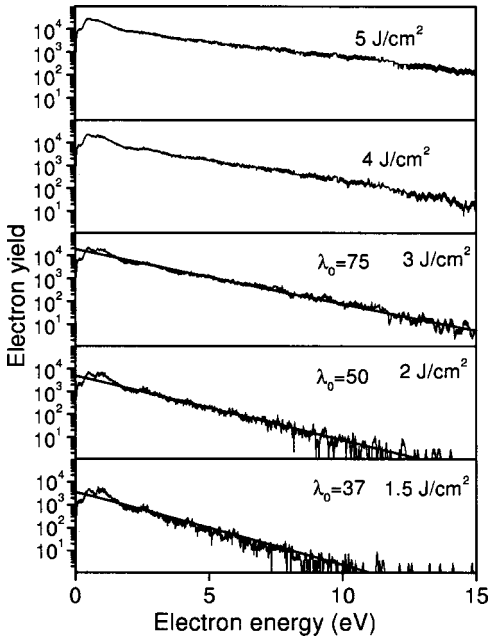

FIG. 4. Examples of distributions of measured electron kinetic energy for laser pulse durations of 180 fs at different pulse energies. Also shown are examples of calculated distributions according to the formula derived in the main text. The average photon number absorbed in the center of the laser beam ($\sigma_{ph}F_0/h\nu$) is indicated. For the two highest fluences no theoretical curve was calculated due to the lifetime broadening effect discussed in the main text.

absorbed photons. The relation between the laser fluence and the slopes of the curves in the figure will be discussed below.

B. Apparent electron temperatures

Both the experimental and theoretical electron kinetic energy spectra have a form which resembles a Boltzmann distribution very closely,

$$P(\varepsilon) \propto e^{-\varepsilon/T_a}, \tag{10}$$

where T_a has dimension of temperature (we will set $k_B = 1$). One can understand this in terms of the rate constant Eq. (1) and the capture cross section Eq. (5), which predict this behavior for small ε;

$$k(E,\varepsilon)d\varepsilon \propto \rho_d(E-\Phi-\varepsilon)d\varepsilon \approx \rho_d(E-\Phi)e^{-\varepsilon/T_d}d\varepsilon \tag{11}$$

with T_d defined as the microcanonical temperature,[18]

$$T_d^{-1} \equiv \frac{d\ln(\rho_d(E_0-\Phi))}{dE}. \tag{12}$$

This expression is approximate since the spectra contain electrons emitted by molecules with a range of different excitation energies, i.e., with different values of T_d. The identification of the reciprocal of the slope of the logarithm of the electron energy spectra with a microcanonical temperature is therefore not rigorous. Nevertheless, it is convenient to analyze the data with this fit parameter since it both gives an indication of the magnitude of the microcanonical temperature of the product molecule(s), and provides a robust comparison of experiment and theory.

The apparent electron temperatures, T_a, have been fitted from both the experimental data and the simulated spectra

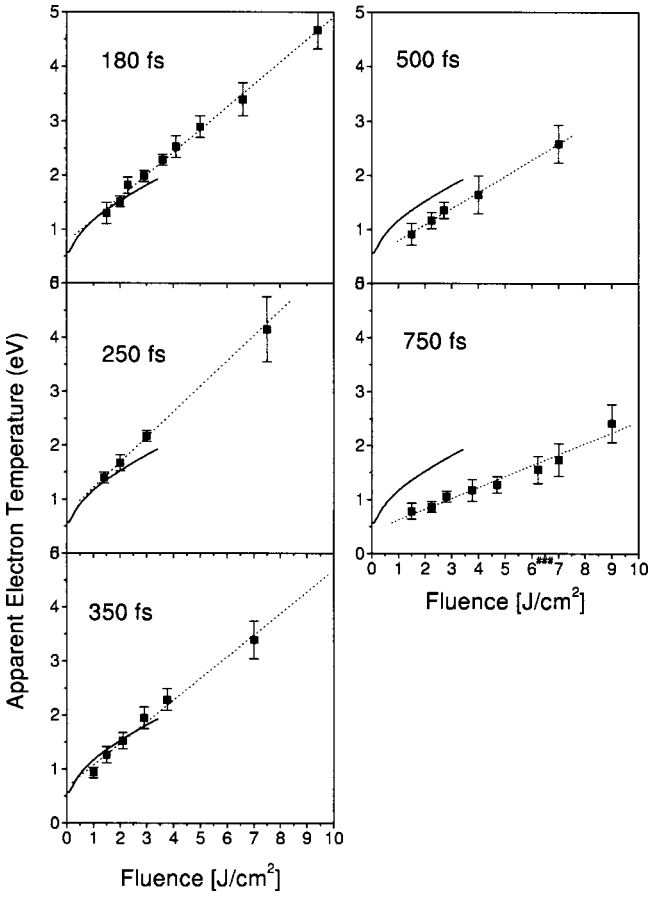

FIG. 5. Fitted apparent electron temperatures from electron kinetic energy spectra recorded with pulse duration from 180 fs to 750 fs (squares). T_a increases roughly linearly with laser fluence, although a small negative curvature may be present for the short pulses. The full line is the simulated values of T_a for a negligibly short laser pulse (compared to τ).

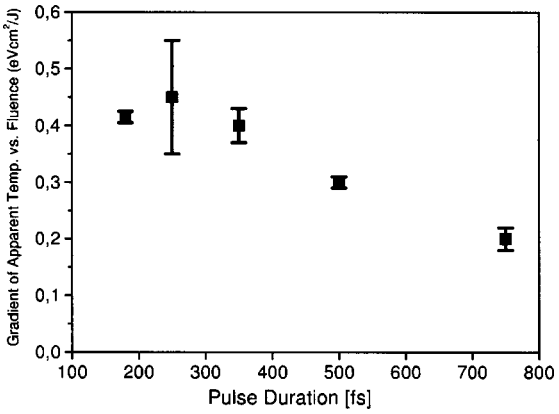

FIG. 6. Gradients of apparent temperature vs fluence (Fig. 5), plotted vs excitation laser pulse duration. The decrease beyond 300 fs indicates the time constant for coupling of the electronic energy to vibrational degrees of freedom.

generated as described above. The results of the fits are shown versus laser fluence for different pulse durations in Fig. 5.

The plots also show the corresponding theoretical curve for a laser pulse of negligible duration, i.e., the values fitted from the curves shown in Fig. 3. The conversion from the number of absorbed photons to laser fluence has been accomplished by using a cross section of 0.12 Å^2, which is the only fit parameter for this curve. This can be thought of as an average absorption cross section for absorbing many 800 nm photons and should not be considered the same as the cross section for absorption of a single photon in the ground state C_{60}.

Note that the uncertainty in the absolute value of the experimental laser fluence is rather large ($\pm 50\%$). The experimental fluence is calculated as $F=E/(\pi w^2)$, where E is the pulse energy and w the beam radius of 25 μm. The fluence in the center of the laser beam, F_0, and the experimental fluence, F, are connected by the relation

$$E=\int 2\pi r\, dr F_0 e^{-r^2/2w^2}=2\pi w^2 F_0, \tag{13}$$

and hence $F_0=F/2$. This conversion will be used throughout the paper. The theoretical curve reproduces the experimental data up to approximately 3 J/cm^2, which corresponds to an average number of photons absorbed in the center of the laser beam of 75, as calculated with the above photo absorption cross section. At this energy the calculated rate constant exceeds 10^{16} s^{-1}. The lifetime of the levels used to calculate the level density must be less than the reciprocal of this value if the electron emission is statistical, and consequently the levels will be broadened by the Heisenberg time-energy uncertainty relation by at least the amount corresponding to this time. Hence also the level density will be modified, by a smearing which will make the curve less steep. This influences the apparent electron temperature directly, as can be seen from Eq. (6), and will produce apparent temperatures which are too high. For the specific example, the lifetime broadening of the single levels is a few times the measured apparent temperature.

Based on these considerations we expect that the value of the cross section from this estimate is on the high side. A quantitative analysis of the lifetime broadening is complicated, not least due to the finite duration of the laser pulse, and will not be attempted here.

The measurements of the apparent electron temperature at different pulse durations shown in Fig. 5 give an indication of the electron-phonon coupling time. The fluence dependences are reasonably straight lines with approximately the same (finite) intercept with the ordinate. The data can therefore be represented by the value of the slope. These are plotted in Fig. 6, which shows a significant variation with pulse duration, with a clear decrease in the value after a few hundred fs. This provides a direct, albeit not very precise, measurement of the energy dissipation time constant.

A more precise value is provided by the pump–probe experiments mentioned in the introduction. Another indicator for the coupling time are earlier data on the threshold laser pulse duration for the appearance of the delayed ionization tail in positive ion mass spectra.[7] Delayed ionization can be detected when sufficient electronic excitation energy has been transferred to the vibrational degrees of freedom to allow thermionic emission on the microsecond time scale. This was found to lie in the range of 500–750 fs, depending on the laser fluence.[7] As is the case for the data in Fig. 6, we expect that value to overestimate the coupling time relative

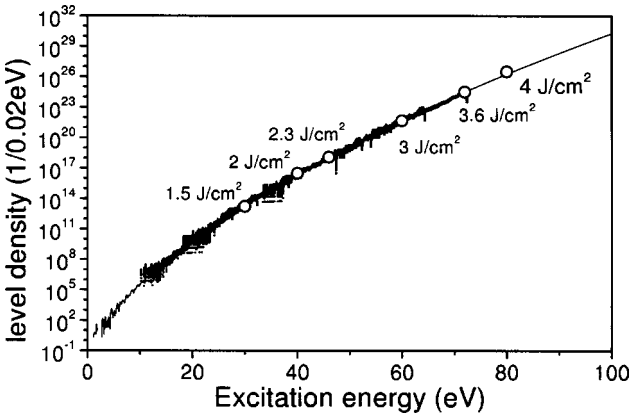

FIG. 7. Theoretical level densities of C_{60}^+ (line), electron energy distributions plotted as described in the text (dots), and the corresponding electronic level density of the parent C_{60} (open circles). The fluences used for the experimental spectra are indicated at the symbol for the parent level density.

to the pump–probe experiments, but a detailed quantitative analysis of the long pulse duration data will not be attempted here.

C. Level density of C_{60}^+; comparison with experiments

If Eq. (6) is applied to electron emission from the neutral molecule, which is the dominant contribution to the electron energy distributions for low and medium excitation energies, the equation can be rearranged by isolating the level density of C_{60}^+;

$$\rho_d(E_0-\Phi-\varepsilon)\propto P(E_0,\varepsilon)/(\varepsilon+|V(r_0)|)\rho_p(E_0). \qquad (14)$$

This means that if the observed electron energy distributions, $P(E_0)$, are mirrored around the $\varepsilon=0$-axis and shifted to the energy $E_0-\Phi$, they will provide an image of the level density of the daughter at that energy. The quantities on the right hand side of Eq. (14) are measured directly, apart from the relatively unimportant value of $|V(r_0)|$, and the value of the excitation energy, E_0. If we ignore the complications due to the distributions of excitation energies in the molecule during electron emission, the equation provides a simple relation between the level density of C_{60}^+ and the measured electron energy distributions. The relation includes as a single parameter, the photo excitation energy or, equivalently, the photo absorption cross section. Figure 7 shows the C_{60}^+ level densities calculated with this formula. The average energy absorbed, $F_0\sigma_{ph}$, was calculated with the cross section $\sigma_{ph}=0.06$ Å^2. The convolutions due to Poisson statistics and Gaussian beam profile are not considered, as also the contribution from electrons from higher charge states, and the agreement between the theoretical level density and the measured curves is therefore only suggestive.

The fit also requires a normalization constant. From Eq. (14) it is clear that this number is proportional to the parent level density at the energy E_0, with a constant of proportionality which is independent of E_0 when the experimental data have been properly normalized to the number of laser shots. If we ignore the differences between the level densities of the different charge states, which are small at these energies, we can fit the parent level density to the daughter level density with just a single fit parameter (open circles on the figure). The fit of all curves and points in Fig. 7 therefore only requires a total of two fit parameters, of which one is the cross section. The agreement is very satisfactory.

D. Inclusive ion yields

The yield of ions depends strongly on the laser fluence and on the pulse duration. Also here we will consider only short pulses. Then the ion yields are calculated with application of the same physics and basic formulas as the electron energy distributions used above. Both singly and doubly charged molecules are created,

$$C_{60}\rightarrow C_{60}^+ + e^-, \quad C_{60}^+\rightarrow C_{60}^{2+} + e^-. \qquad (15)$$

Smaller amounts of triply and quadruply charged cations are formed, and the amount can be calculated in analogy to the population of the doubly charged molecule, described below. The molecules, singly or multiply charged alike, may undergo fragmentation at a later stage, depending on the amount of energy absorbed. The total yield of all ions can be calculated with the model as that of the yield of C_{60}^+, when further ionization and fragmentation are ignored, since every ion, irrespective of mass or charge state, will be created initially as C_{60}^+. The expression for this yield is given in Eq. (3). When multiply charged species and fragments appear, it generalizes to

$$\sum_{q\geq 1,N\leq 60} Y(C_N^{q+}) = 1-\exp\left(-\int_0^\infty k(E(t))dt\right). \qquad (16)$$

This expression gives the theoretical total ion yield and can be compared with the experimentally measured total ion yield, avoiding all complications due to fragmentation. The comparison between experimental and theoretical curves is shown in Fig. 8. The curves agree quite well with the chosen cross section of 0.024 Å^2.

E. Singly/doubly charged ion yields

A comparison of the experimental and the calculated ratio between the singly and the doubly charged C_N can also be used to set the energy scale and thus provide yet another estimation of the absorption cross section. We expect it to be a little less accurate than the method of the previous section because the ion in the relatively weak doubly charged ion signal may be more prone to subsequent fragmentation than the singly charged species, or may fission which is a channel which is not open to singly charged species. There are also uncertainties related to the correction for different ion detection efficiencies.[29]

The ion yield for the different charge states can be calculated by considering ionization beyond the first. As an example we give the procedure for the calculation of the ion abundance for doubly and higher charged ions.

The distribution of internal energy of the singly ionized species, $p(E)$, is determined as

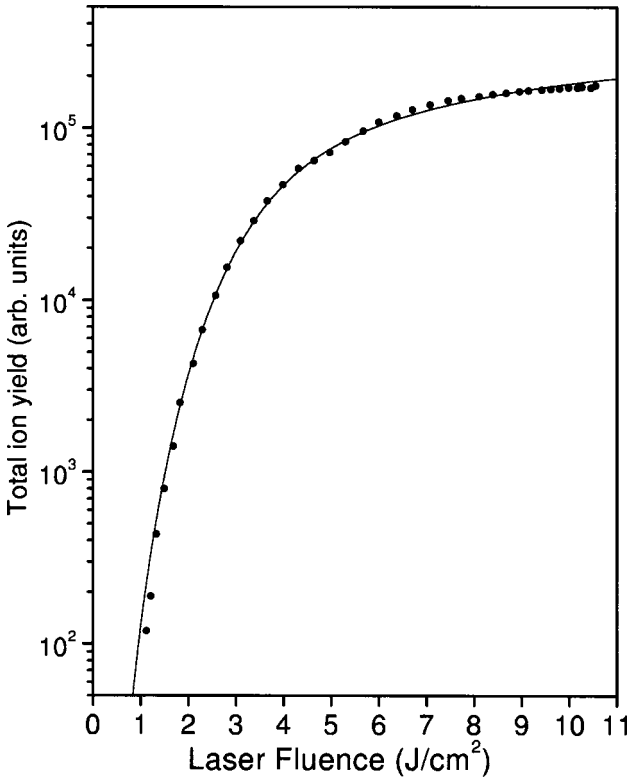

FIG. 8. Total ion yield vs laser fluence. The theoretical curve is converted to fluence, assuming a photon absorption cross section of 0.024 Å^2.

$$dp(nh\nu e^{-t/\tau}-\Phi-\varepsilon) = dtk(nh\nu e^{-t/\tau},\varepsilon)\exp\left(-\int_0^t k(nh\nu e^{-t'/\tau})dt'\right). \quad (17)$$

The first factor is the rate constant given by Eqs. (1), and the second is the surviving fraction. The distribution thus calculated is the distribution of internal (electronic) excitation energies immediately after the first electron has been emitted. Adding contributions from all possible kinetic energies and summing over the number of absorbed photons and the fluence variations over space proceeds as in the previous section [Eqs. (8) and (9)] and results in a distribution of singly charged molecules with different electronic excitation energies. Once this distribution, $p(E)$, is calculated it can be used for the calculation of the total yield of C_{60}^{q+};

$$Y(C_{60}^{q+}) = \int_0^\infty dE p(E)(1-e^{-\int_0^\infty dt k_2(Ee^{-t/\tau})}), \quad q \geqslant 2. \quad (18)$$

The rate constant k_2 is the one pertaining to the second of the emission processes in Eq. (15), with an activation energy of 11.4 eV, and a functional form discussed in Sec. IV A.

The calculation of the yield of triply and higher charged species proceeds in complete analogy to the calculation of the doubly and higher charged. The total yield of singly resp. doubly charged species can then be expressed as

$$Y(C_N^+) = Y(C_N^{q+})(q \geqslant 1) - Y(C_N^{q+})(q \geqslant 2), \quad (19)$$

$$Y(C_N^{2+}) = Y(C_N^{q+})(q \geqslant 2) - Y(C_N^{q+})(q \geqslant 3). \quad (20)$$

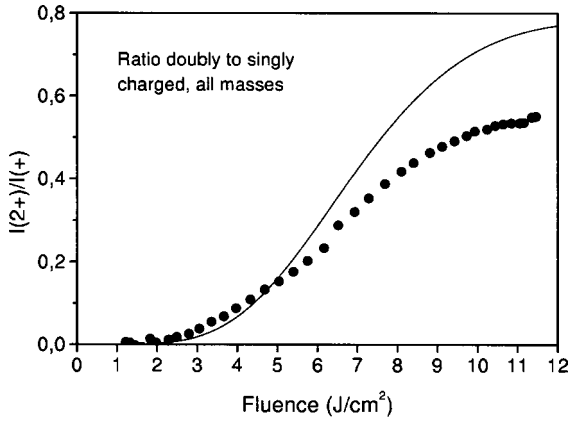

FIG. 9. The ratio of the ion counts of all doubly charged fullerenes to singly charged vs laser fluence. The theoretical curve has been scaled with a photon cross section of 0.012 Å^2. The absolute count of doubly charged species spans about four orders of magnitude over the fluences covered in the plot.

The measured dimer-monomer ratio is shown in Fig. 9 versus laser fluence together with the theoretical curves based on formulas of the previous section. The only adjustable parameter is the scaling of the abscissa of the theoretical curve. The agreement is not unreasonable.

The abundance of all ionized C_N with charge from $+1$ to $+4$ was calculated with the above procedure for a number of different fluences. The calculated values are shown in Fig. 10. For low fluences, up to $\lambda_0 = 6-7$, the different charges follow a power law in fluence to a very good approximation. Interestingly, the powers are 4.95, 12.3, 22.9, and 35.9 for charges $+1$ through $+4$. These numbers compare very well with the ratios of accumulated ionization energies, calculated in units of the photon energy, viz. 4.88, 12.2, 23.0, and 35.9. The agreement cannot be fortuitous but at present the reason for it is not clear to us. One lesson from this is that, contrary to established practise, the observation of a power dependence in fluence is not sufficient to allow one to conclude that a process occurs via direct multiphoton absorption.

Another interesting point to observe is, that all yields in Fig. (9) tend towards a limiting value. This is seen most

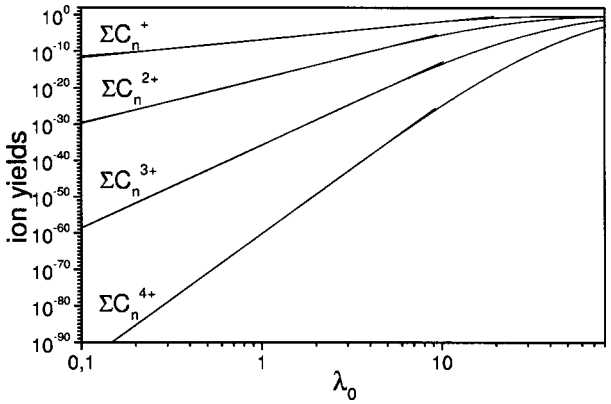

FIG. 10. The theoretical total ion yields vs fluence for charge states 1+ to 4+. The yields plotted are calculated as those of C_{60}^{n+}. Comparison with experiments require a summation of all experimentally observed fragments with the same charge state. The figures also contains the (hardly visible) fitted power laws.

easily for the singly and doubly charged species. This behavior is somewhat surprising, since one would expect a decrease at sufficiently high laser fluence, but has a simple explanation in terms of the laser beam profile. The energies which give rise to the singly charged species, say, but which are not sufficient to cause the second ionization, are effectively limited both from above and below, so that practically all singly charged species are generated from molecules which have absorbed a minimum number of photons and less than a maximum number. By the Poisson statistics, these two limits translate into a more or less well-defined interval of laser fluences. When the total pulse energy is increased, this ring-shaped interval moves radially outwards. For a Gaussian beam profile, the width of the ring is reduced in radial extension by the reciprocal of the radius. At the same time the circumference is increased with an amount proportional to the increase in radius. The net result is that the area of the laser beam which will produce singly ionized species is conserved, and consequently that the amount of singly charged molecules saturate. This explanation can be made more quantitative and is not specific to either C_{60} or experiments with fs lasers. It has consequences for conclusions drawn from photo fragmentation experiments on clusters and will be the subject of a future publication.[30]

V. SUMMARY AND CONCLUSIONS

We have fitted total electron yields from Penning ionization data with a transient thermal emission model. The electron-phonon coupling time was found to be about 240 fs. This value agrees well with measurements of photoelectron spectra with varying excitation laser pulse durations. Photoelectron spectra were fitted and the quasi-Boltzmann behavior of the electron spectra was reproduced. Total ion yields were reproduced. Doubly to singly charged intensities were reproduced. Level densities were related to measured electron energy distributions and showed good agreement with the theoretically calculated ones. All these data provided a fit of the photon absorption cross section, which, apart from an instrumental parameter, was the only fit parameter.

The absolute, average photo absorption cross sections fitted from the four different types of data span a factor of 10 from the smallest to the largest. The geometric mean is 0.04 $Å^2$ and the uncertainty on the mean a factor two. As a determination of the absolute magnitude of an indirectly measured cross section this seems like a decent result to us, and we find that the approximate agreement corroborates the fits from which the values have been derived. But the agreement is obviously not completely satisfactory. The differences between the four values can have several reasons. The values from the electron spectra (0.12 and 0.06 $Å^2$) differ by a factor 2, as do the ones from the ion data (0.024 and 0.012 $Å^2$). The higher fitted cross section for the electron spectra data could possibly be explained as the result of a partial equilibration of the electron system, due to a finite electron-electron coupling time. In this case, the electron temperature would be higher than for a totally equilibrated system. In the fit this will appear as a higher cross section. Alternatively one can ascribe the difference in electron- and ion-data to a real difference in the level density of the charged species from the form used for the fit. Differences between true and assumed forms can obviously vary also with the charge state of the molecule and need not be identical for all charged species. It should be noted that the electron spectra data measure essentially the slope of the level density and the ion yield data the total yield or ratios of total yields, which involves absolute rates. Of experimental uncertainties one should mention the day-to-day reproducibility of the laser beamwaist, which is estimated at 50%. Shot-to-shot fluctuations in laser power are not considered, either. For the doubly-singly ionized ratio, which gives the lowest fitted cross section, one can speculate to what extent the doubly charged species are depleted from the beam by fissionlike processes. These will tend to remove the doubly charged molecules but not the singly charged since those do not fission. This will reduce the measured ratio and tend to give a cross section which is underestimated, consistent with the low fitted value. The precise effect of these, mainly systematic, uncertainties are difficult to quantify without embarking on a major computational study of the data, and that may even not provide conclusive results. We suspect that several possible explanations are consistent with the data and believe that a resolution of which ones are right will need further experimental input.

The theoretical fluence dependencies were found to exhibit power dependencies with powers very close to the accumulated ionization energies of the species.

Remaining open are the theoretical questions of how to deal with the level density at high rates where lifetime broadening is important, of the behavior at laser pulses longer than the electron-phonon coupling time, and to give a more detailed mechanism for the electron-phonon coupling.

ACKNOWLEDGMENTS

This work has been supported by the European Community—Access to Research Infrastructure action of the Improving Human Potential Program, the EU Network ''Delayed Ionization and Competing Cooling Mechanisms in Atomic Clusters'' (HPRN-CT-2000-00026) and the Deutsche Forschungsgemeinschaft via SFB 450 ''Analyze und Steuerung ultraschneller photoinduzierte Reaktionen.'' The authors thank former colleagues at the Max-Born-Institut, G. Korn, M. Wittmann and H. Rottke for their help with the experiments and I.V. Hertel for his support of the project. K.H. thanks S.A. Hansen for stimulating conversations, E.C. thanks R.D. Levine for many fruitful discussions on this topic.

APPENDIX: CALCULATION OF C_{60} ELECTRONIC LEVEL DENSITIES

This Appendix gives the recipe which was used to calculate the electronic level densities of all charge states of C_{60} in this work. The algorithm is similar to the one given by Williams[31] and requires only a set of independent particle states as input.

Denoting the level density at energy E of the system composed of n electrons and $n_l(>n)$ single particle states by $\rho(n,n_l,E)$, the following recurrence relation holds:

$$\rho_f(n,n_l,E)=\rho_f(n,n_l-1,E)+\rho_f(n-1,n_l-1,E-E_l), \tag{A1}$$

where E_l is the energy of level l. This corresponds to a decomposition of ρ into the part which sums up all the states where level l is unoccupied and the part which sums up all states where level l is occupied and the remaining $n-1$ electrons are distributed over the other $l-1$ levels. The last part is to be evaluated at energy $E-E_l$ since the energy E_l is used to occupy level l. If $E-E_l<0$ ρ is zero. The summation is initialized by calculating $\rho(1,n_l,E)$ directly.

The computing time varies as $n_e(n_s-n_e)E/\delta E$, where n_e is the total number of electrons, n_s the total number of levels, E is the highest excitation energy and δE is the energy resolution.

[1] E. E. B. Campbell, G. Ulmer, and I. V. Hertel, Phys. Rev. Lett. **67**, 1986 (1991).
[2] B. A. Collings, A. W. Amrein, D. M. Rayner, and P. A. Hackett, J. Chem. Phys. **99**, 4174 (1993).
[3] G. Ganteför, W. Eberhardt, H. Weidele, D. Kreisle, and E. Recknagel, Phys. Rev. Lett. **77**, 4524 (1996).
[4] E. E. B. Campbell and R. D. Levine, Annu. Rev. Phys. Chem. **51**, 65 (2000).
[5] J. U. Andersen, E. Bonderup, and K. Hansen, J. Phys. B **35**, R1 (2002).
[6] E. E. B. Campbell, K. Hansen, K. Hoffmann, G. Korn, M. Tchaplyguine, M. Wittmann, and I. V. Hertel, Phys. Rev. Lett. **84**, 2128 (2000).
[7] E. E. B. Campbell, K. Hoffmann, and I. V. Hertel, Eur. Phys. J. D **16**, 345 (2001).
[8] K. Hansen, Proceedings of 'Similarities and Differences Between Atomic Nuclei and Clusters,' Tsukuba, Japan, July 1997 (Y. Abe, I. Arai, S. M. Lee, K. Yabana, Eds.) AIP Conf. Proc., New York (1998).
[9] J. M. Weber, K. Hansen, M.-W. Ruf, and H. Hotop, Chem. Phys. **239**, 271 (1998).
[10] R. Schlipper, R. Kusche, B. von Issendorf, and H. Haberland, Appl. Phys. A: Mater. Sci. Process. **72**, 255 (2001).
[11] M. Maier, M. Astruc Hoffmann, and B. von Issendorff, New J. Phys. **5**, 3.1 (2003).
[12] J-Y. Bigot, V. Halte, J.-C. Merle, and A. Daunois, Chem. Phys. **251**, 181 (2000).
[13] M. Perner *et al.*, Phys. Rev. Lett. **78**, 2192 (1997).
[14] H. Inouye, K. Tanaka, I. Tanahashi, and K. Hirao, Phys. Rev. B **57**, 11334 (1998).
[15] B. Brunetti, P. Candori, R. Ferramosche, S. Falcinelli, F. Vecchiocattivi, A. Sassara, and M. Chergui, Chem. Phys. Lett. **294**, 584 (1998).
[16] E. E. B. Campbell, K. Hoffmann, H. Rottke, and I. V. Hertel, J. Chem. Phys. **114**, 1716 (2001).
[17] C. Voisin, D. Christofilos, N. Del Fatti, F. Valle, B. Prével, E. Cottancin, J. Lerme, M. Pellarin, and M. Broyer, Phys. Rev. Lett. **85**, 2200 (2000).
[18] J. M. Blatt and V. F. Weisskopf, *Theoretical Nuclear Physics* (Dover, New York, 1979).
[19] K. Hansen, Philos. Mag. B **79**, 1413 (1999).
[20] R. E. Stanton and M. D. Newton, J. Phys. Chem. **92**, 2141 (1988).
[21] C. E. Klots, Chem. Phys. Lett. **186**, 73 (1991).
[22] K. Hansen and E. E. B. Campbell, Phys. Rev. E **58**, 5477 (1998).
[23] K. Yabana, private communication.
[24] M. Boyle, K. Hoffmann, C. P. Schulz, I. V. Hertel, R. D. Levine, and E. E. B. Campbell, Phys. Rev. Lett. **87**, 273401 (2001).
[25] D. Ding, R. N. Compton, R. E. Haufler, and C. E. Klots, J. Phys. Chem. **97**, 2500 (1993).
[26] V. Kasperovich, G. Tikhonov, and V. V. Kresin, Chem. Phys. Lett. **337**, 55 (2001).
[27] M. Boyle *et al.* (unpublished).
[28] M. Tchaplyguine, K. Hoffmann, O. Duhr, H. Hohmann, G. Korn, H. Rottke, M. Wittmann, I. V. Hertel, and E. E. B. Campbell, J. Chem. Phys. **112**, 2781 (2000).
[29] E. E. B. Campbell, G. Ulmer, B. Hasselberger, H.-G. Busmann, and I. V. Hertel, J. Chem. Phys. **93**, 6900 (1990).
[30] K. Mehlig *et al.* (unpublished).
[31] F. C. Williams, Nucl. Phys. A **133**, 33 (1969).